nature communications



Article

https://doi.org/10.1038/s41467-025-63042-9

Topological phonon blockade and its transfer via dark-mode engineering

Received: 24 November 2024

Deng-Gao Lai ¹ □ Adam Miranowicz ^{1,2} & Franco Nori ^{1,3}

Accepted: 7 August 2025

Published online: 29 August 2025

Check for updates

Unidirectional topological behavior, engendered by imposing topological operations winding around an exceptional point, is sensitive to dark modes, which allow deactivating topological operations, resulting in a complete blockade of both mode conversion and phonon transfer between dark and bright modes. Here we demonstrate how to beat this challenge and achieve a versatile vet unique nonreciprocal topological phonon transfer and blockade via dark-mode engineering. This happens by harnessing the power of synthetic magnetism, leading to an extraordinary transition between the dark-mode nonbreaking and breaking regimes, in a precise and controlled manner. Specifically, topological phonon blockade (transfer) happens in the dark-mode nonbreaking (breaking) regime, offering an exciting opportunity of switching between topological phonon blockade and its transfer on demand, which has no counterpart in previous studies. Remarkably, applying dark-mode engineering to quantum optomechanical networks can enable scalable network-based topological phonon transfer and quantum collective ground-state preparation. The proposed mechanism has general validity and can be generalized to the manipulation of various dark-state-related quantum effects, advancing the development of scalable quantum information processors. This study maps a general path towards generating a profoundly different topological quantum resource with immunity against both dark modes and dark states.

Nontrivial topology, mainly governed by non-Hermitian degeneracies¹⁻¹⁹, has led to various counterintuitive and fascinating topological types of behavior by adiabatically encircling exceptional points (EPs) in parameter spaces, such as chiral phase accumulation^{20,21}, non-adiabatic jumps^{22,23}, and topological phonon transfer (TPT) or mode conversion²⁴⁻³⁴. These topological phenomena, however, are generally destroyed by dark modes, which are naturally decoupled from systems³⁵⁻⁴⁰, resulting in a complete malfunction of both EPs and topological operations. For example, TPT and mode switching can always happen when executing adiabatic closed paths enclosing an EP^{24,25}. Surprisingly, if a system exhibits dark modes, both mode conversion and TPT between dark and bright modes are unfeasible, regardless of the adjustment of adiabatic trajectories and

system parameters, due to the dark-mode-induced destruction of topological operations and EPs.

Previously established topological achievements in theories and experiments are focused exclusively on conventional scenarios²⁰⁻³⁴, where dark modes are entirely circumvented because topological responses are usually diminished by dark modes^{24,25}. Nevertheless, the practical applicability of modern topological quantum technologies has challenged such progress by demonstrating that a universal approach must be explored for confronting this challenge posed by dark modes, rather than evading it^{41–50}. In view of its significance, exploiting a fundamentally different topology immune to dark modes, as well as shielding both EPs and topological operations from dark-mode disturbances in practical devices, is highly desirable.

¹RIKEN Center for Quantum Computing (RQC), 2-1 Hirosawa, RIKEN Wako-shi, Saitama, Japan. ²Institute of Spintronics and Quantum Information, Faculty of Physics and Astronomy, Adam Mickiewicz University, Poznań, Poland. ³Physics Department, University of Michigan, Ann Arbor, MI, USA.

e-mail: denggaolai@foxmail.com

Here, we show how to address this long-standing challenge and achieve a profoundly different one-way TPT, unveiling its counterintuitive immunity against dark modes. This occurs because of the synergy of topological operations ^{24,25} and synthetic magnetism ⁵¹⁻⁶³, resulting in an exceptional transition between dark-mode-nonbreaking (\mathcal{DMN}) and dark-mode-breaking (\mathcal{DMB}) regimes in a well-controlled manner. Note that a reconfigurable synthetic gauge field has recently been demonstrated in phase-dependent loop-coupled optomechanical configurations ⁵¹⁻⁶³.

We reveal that executing a topological operation in the \mathcal{DMN} regime yields topological phonon blockade (TPB) between dark and bright modes; whereas performing it in the \mathcal{DMB} regime allows TPT. This enables a versatile yet unique topological physics and provides an exciting possibility of bridging TPB and TPT at will, which is otherwise unattainable in previously established demonstrations^{20–34}. Unlike previous approaches, where both EPs and topological operators are entirely malfunctioning due to dark modes^{20–34}, our approach is entirely immune to this detrimental inactivation effect.

The dark-mode-engineering mechanism is universal, and it can be extended to break various dark-state effects in quantum physics and to beat the limitation⁴⁰, where dark modes prevent conventional quantum control and ground-state preparation. Our findings could advance the control of quantum collective motion in macroscopic mechanical systems⁴⁰ and the development of scalable quantum information processors utilizing excitations, with potential applications in state or energy manipulation, pulse generation, and the conversion of quantum information^{64–67}. In a broader view, our study sheds light on the combination of dark-mode engineering, topological operations, and quantum networks, and offers an exciting prospect of revealing a unique quantum topology immune to dark modes (states).

Results

System and dark-mode engineering

We focus on a three-mode optomechanical system, consisting of two phonon modes coupled to a common photon mode through radiation-pressure interaction, as shown in Fig. 1a. The described system has already been implemented using state-of-the-art technology to achieve topological responses fully evading dark modes²⁴. The system Hamiltonian reads ($\hbar = 1$)

$$\mathcal{H} = \omega_{c} a^{\dagger} a + \sum_{j=1,2} \left[\omega_{j} b_{j}^{\dagger} b_{j} + g_{j} a^{\dagger} a (b_{j}^{\dagger} + b_{j}) \right]$$

$$+ i \sqrt{\kappa_{\text{in}}} \epsilon_{\text{in}} (a^{\dagger} e^{-i\omega_{L} t} - \text{H.c.}) + \mathcal{H}_{\xi},$$

$$\mathcal{H}_{\xi} = \xi (e^{i\Theta} b_{1}^{\dagger} b_{2} + e^{-i\Theta} b_{2}^{\dagger} b_{1}),$$

$$(1)$$

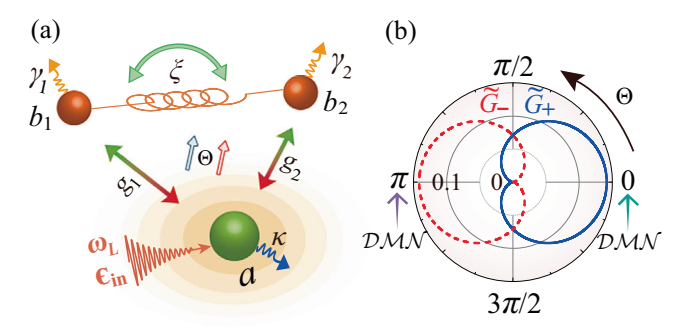


Fig. 1 | **Physical model and dark-mode control.** a Schematic of synthetic-magnetism-engineered quantum devices, consisting of a photon mode a (with damping rate κ) optomechanically coupled to two phonon modes b_j (with decay rates γ_j and coupling strengths g_j), both of which are coupled to each other via a phase-dependent phonon-hopping interaction (ξ and Θ). **b** Effective coupling strengths \tilde{G}_{\pm} versus Θ , when introducing synthetic magnetism. Simply tuning $\Theta = n\pi$ and $\neq n\pi$ for an integer n leads to a dark mode $(\tilde{G}_{\pm} = 0, \mathcal{DMN})$ regime) and

where a (a^{\dagger}) and b_j (b_j^{\dagger}) are the annihilation (creation) operators of the photon and jth phonon modes with resonance frequencies ω_c and ω_j , respectively. The g_j term is the light-motion interaction, and the $\epsilon_{\rm in} = \sqrt{P/(\hbar\omega_L)}$ term denotes the laser driving with power P, frequency ω_L , and input-coupling rate $\kappa_{\rm in}$. Synthetic gauge fields^{51–63}, employed for manipulating the dark mode, can be induced using a phase-dependent loop-coupling setup formed by the g_j and \mathcal{H}_{ξ} terms (with phonon-hopping coupling strength ξ and modulation phase Θ) (see Supplementary Information). Note that in the absence of synthetic magnetism ($\xi = 0$), our system naturally reverts to the conventional case²⁴, associated with the \mathcal{DMN} regime.

To explore how the dark mode is engineered by the synthetic gauge field, we derivate the linearized Hamiltonian, $\mathcal{H}_{\text{lin}} = -\Delta\delta a^{\dagger}\delta a + \sum_{j=1,2} [\omega_j \delta b_j^{\dagger}\delta b_j + G_j (\delta a \delta b_j^{\dagger} + \text{H.c.})] + \xi(e^{i\Theta}\delta b_1^{\dagger}\delta b_2 + \text{H.c.})$, with Δ and G_j being the driving detuning and linearized photon-phonon coupling strength, respectively (see Supplementary Information for detailed derivations). This is achieved by applying a linearization procedure and expanding all operators $o \in \{a, b_j, a^{\dagger}, b_j^{\dagger}\}$ as sums of their classical averages and quantum fluctuations, i.e., $o = \bar{o} + \delta o$. Without synthetic magnetism (i.e., $\xi = 0$), the bright (\mathcal{B}_+) and dark (\mathcal{B}_-) modes emerge when $\omega_j = \omega_m$:

$$\mathcal{B}_{+} = (G_1 \delta b_1 + G_2 \delta b_2)/G_0, \text{ bright,}$$
 (2a)

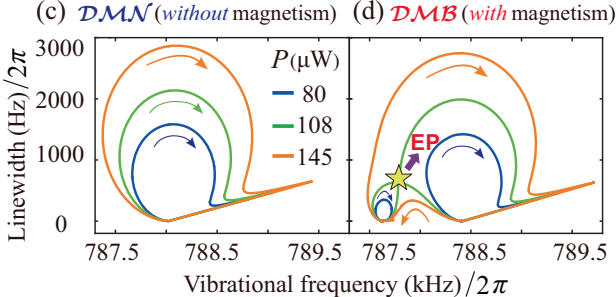
$$\mathcal{B}_{-} = (G_2 \delta b_1 - G_1 \delta b_2) / G_0, dark, \tag{2b}$$

with $G_0 = \sqrt{G_1^2 + G_2^2}$. The dark mode is completely decoupled from the system, resulting in a complete blockade of both mode conversion and phonon transfer between the dark and bright modes^{24,25}.

Surprisingly, this dark mode can be controlled at will by simply employing synthetic magnetism (i.e., $\xi \neq 0$ and $\Theta \neq 0$). To elucidate the underlying physics behind this counterintuitive phenomenon, two normal modes associated with synthetic magnetism are introduced as: $\tilde{\mathcal{B}}_{\pm} = \mathcal{F}\delta b_{1(2)} \mp e^{\pm i\Theta} \mathcal{K}\delta b_{2(1)}$, where $\mathcal{F} = |\delta \tilde{\omega}_{-}|/\sqrt{(\delta \tilde{\omega}_{-})^2 + \xi^2}$ and $\mathcal{K} = \xi \mathcal{F}/\delta \tilde{\omega}_{-}$, with $\delta \tilde{\omega}_{-} = \tilde{\omega}_{-} - \omega_{1}$ and $\tilde{\omega}_{\pm} = (\omega_{1} + \omega_{2} \pm \sqrt{(\omega_{1} - \omega_{2})^2 + 4\xi^2})/2$. Subsequently, the linearized Hamil-

tonian becomes $\mathcal{H}_{\text{lin}} = -\Delta \delta a^{\dagger} \delta a + \sum_{l=\pm} [\tilde{\omega}_l \tilde{\mathcal{B}}_l^{\dagger} \tilde{\mathcal{B}}_l + (\tilde{G}_l \tilde{\mathcal{B}}_l \delta a^{\dagger} + \text{H.c.})]$, with the effective coupling strengths:

$$\tilde{G}_{+} = \mathcal{F}G_{1(2)} \mp e^{\mp i\Theta} \mathcal{K}G_{2(1)}. \tag{3}$$



its breaking $(\bar{G}_{\pm} \neq 0, \mathcal{DMB}$ regime), respectively. We set $\omega_{j}/\omega_{m} = 1$ and $G_{j}(\xi)/\omega_{m} = 0.1$. **c**, **d** Mechanical linewidths and resonance frequencies versus the driving power P and detuning $\Delta \in [-1800 \text{kHz}, 0]$, when the system operates in (**c**) the \mathcal{DMN} regime (without synthetic magnetism, i.e., $\xi = 0^{24}$) and (d) the \mathcal{DMB} regime (with synthetic magnetism, i.e., $\xi/\omega_{m} = 5 \times 10^{-4}$ and $\Theta/\pi = 1/9$). The arrows describe the eigenvalue variation with increasing Δ for a fixed P.

We find from Eq. (3) that dark-mode engineering can be realized through two distinct mechanisms: (i) synthetic magnetism and (ii) asymmetric coupling. In the following, we provide a detailed elucidation of these two mechanisms.

(i) Synthetic magnetism enables dark-mode engineering. When $G_1 = G_2$, we plot \tilde{G}_\pm versus Θ [see Fig. 1b and Supplementary Fig. S1 for more details], which reveals that for $\Theta = n\pi$, the dark mode decoupled from the system emerges, corresponding to the \mathcal{DMN} regime. Counterintuitively, an effective coupling of the dark mode to the system can be flexibly achieved just by tuning $\Theta \neq n\pi$, resulting in the \mathcal{DMB} regime. The fundamental physics driving these counterintuitive phenomena lies in the fact that a reconfigurable synthetic gauge field is built on demand just by steering Θ in the loop-coupled configuration, enabling an exceptional transition between the \mathcal{DMN} and \mathcal{DMB} regimes.

(ii) Asymmetric coupling provides an alternative pathway for dark-mode engineering. Specifically, we find that for $\Theta=0$, the symmetric coupling $G_1=G_2$ creates a dark mode $\tilde{\mathcal{B}}_-$, entering the \mathcal{DMN} regime; whereas broken symmetry (i.e., asymmetrical coupling $G_1\neq G_2$) fully quenches this dark mode, establishing the \mathcal{DMB} regime.

Rise and fall of an EP

An adiabatic elimination of the photon mode yields an effective Hamiltonian for two phonon modes (see Supplementary Information for detailed derivations):

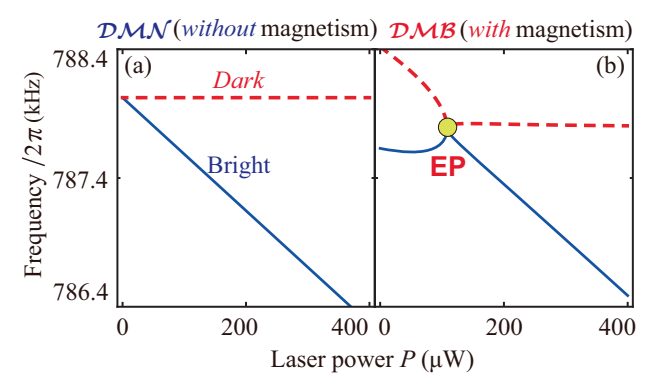
$$\mathcal{H}_{\text{eff}} = \begin{pmatrix} \omega_{1} - \frac{i\gamma_{1}}{2} - ig_{1}^{2}\sigma & \xi e^{i\Theta} - ig_{1}g_{2}\sigma \\ \xi e^{-i\Theta} - ig_{1}g_{2}\sigma & \omega_{2} - \frac{i\gamma_{2}}{2} - ig_{2}^{2}\sigma \end{pmatrix}, \tag{4}$$

where the laser driving induces a complex motional susceptibility σ , defined as

$$\sigma = \frac{P\kappa_{\text{in}}[\chi(\omega_0) - \chi^*(-\omega_0)]}{\hbar\omega_I[(\kappa/2)^2 + \Delta^2]},$$
 (5)

with the driving detuning $\Delta = \omega_L - \omega_c$ and an optical susceptibility $\chi(\omega_0) = [\kappa/2 - i(\omega_0 + \Delta)]^{-1}$, for $\omega_0 = (\omega_1 + \omega_2)/2$. By tuning σ , an EP is easily reached, needing to control over both Im(σ) and Re(σ). Physically, the imaginary and real parts of the corresponding complex eigenvalues correspond to mechanical spectral linewidths and resonance frequencies, respectively. It is enough to tune P and Δ for reaching and encircling this EP, because these parameters are easily manipulated in situ with high precision, timing accuracy, and dynamic range²⁴.

For elucidating the effect of the dark mode on the EP, the mechanical spectra are plotted as functions of Δ and P in both \mathcal{DMN} and \mathcal{DMB} regimes, as depicted in Fig. 1c, d and Supplementary Fig. S2. In the \mathcal{DMN} regime, we show that despite the continuous evolution of the mechanical spectra with system parameters, the EP vanishes at both low and high laser powers, owing to the emergence of the dark



mode [see Fig. 1c]. Counterintuitively, in the \mathcal{DMB} regime, for a lower laser power, each eigenvalue follows an enclosed path, beginning and ending at a same point; while for a higher laser power, both eigenvalues follow open trajectories, each of which ends at the starting point of the other, indicating the emergence of the EP because of breaking the dark mode [see Fig. 1d]. By adjusting Δ and P, the EP [marked by the yellow star in Fig. 1d], where the eigenstates coalesce, appears when the system operates in the \mathcal{DMB} regime, but not in the \mathcal{DMN} regime.

Efficiency of topological phonon transfer

The TPT efficiency \mathbf{F}_+ , which quantifies the phonon transfer from the dark (\mathcal{B}_-) to bright (\mathcal{B}_+) modes, is defined by²⁴

$$\mathbf{F}_{+} = |\mathcal{B}_{+}(\tau)|^{2} / [|\mathcal{B}_{+}(\tau)|^{2} + |\mathcal{B}_{-}(\tau)|^{2}], \tag{6}$$

indicating the fraction of the remaining energy in the bright mode after executing the adiabatic closed control loops, with $|\mathcal{B}_{\pm}(\tau)|$ denoting the amplitudes of the bright and dark modes at the end of the control loops (see Supplementary Information for detailed derivations). This definition of \mathbf{F}_+ must satisfy the property that before performing the control loops, all energy is preserved in the dark mode. Equation (6) clearly shows that (i) a perfect TPT from the dark to bright modes happens when $\mathbf{F}_+=1$, and (ii) a TPB from the dark to bright modes is observed when $\mathbf{F}_+=0$. For ensuring the system stability, the following experimentally feasible parameters are chosen in our simulations²⁴: $g_{1(2)}/2\pi=1.03$ (2.84) Hz, $\kappa(\kappa_{in})/2\pi=177$ (70) kHz, $\omega_{il}/2\pi=788.024$ kHz, and $\gamma_{1(2)}/2\pi=0.6$ (1.4) Hz.

Inactivation and activation of topological operations

When the system operates in the \mathcal{DMN} and \mathcal{DMB} regimes, we display the resonance frequencies and decay rates of mechanical normal modes versus a narrow range of the laser power P (see Fig. 2 and Supplementary Fig. S3). In the \mathcal{DMN} regime, only the bright mode evolves with P, while the dark mode remains invariant, irrespective of the adjustment of system parameters, resulting in a completely deactivation of both the EP and topological operations [Fig. 2a]. This effect enables a complete blockade of the mode conversion and phonon transfer between the dark and bright modes. However, in the \mathcal{DMB} regime, both modes evolve simultaneously with P, which leads to the emergence of characteristic features of the EP, enabling the activation of the EP and topological operations [Fig. 2b]. This offers an exciting opportunity for the revival of the mode conversion and phonon transfer between the dark and bright modes.

Specifically, the eigenstates coalesce at a particular value of the control parameters, and in the vicinity of this EP, they display a structure analogous to the Riemann surfaces of a complex square-root function. When executing a closed-loop path by adiabatically varying P and Δ , the generating smooth evolution on the eigenvalue manifold can return to its starting point only if the EP is not enclosed by the loop. In contrast, adiabatically encircling the EP in a closed-loop trajectory induces a

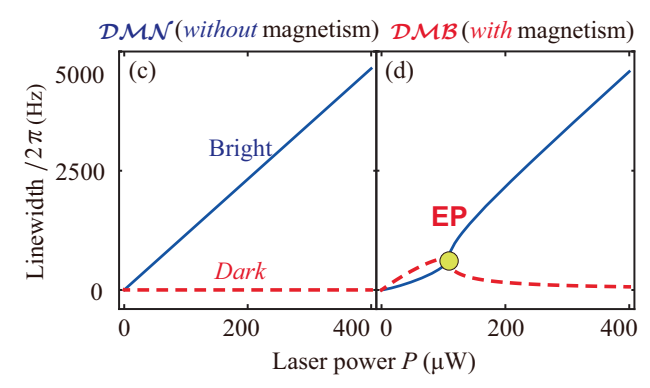
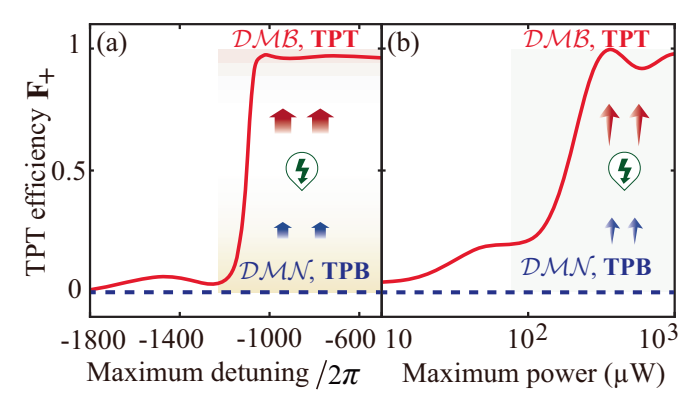


Fig. 2 | Disappearance and appearance of an EP. a, b Resonance frequencies and (c, d) linewidths of mechanical normal modes versus the laser power P in (a, c) the \mathcal{DMN} regime ($\xi = 0^{24}$) and (b, d) the \mathcal{DMB} regime ($\xi/\omega_m = 5 \times 10^{-4}$ and $\Theta/\pi = 1/9$), when $\Delta/2\pi = -847.74$ kHz.



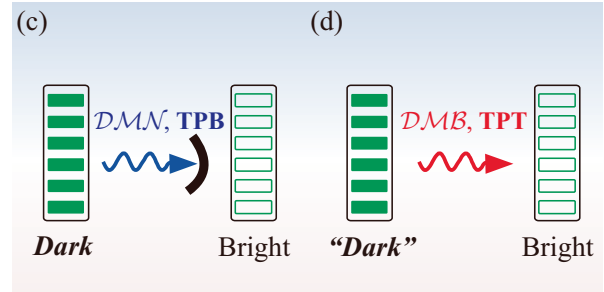


Fig. 3 | Dark-mode-engineered topological phonon transfer and blockade. a, b TPT efficiency \mathbf{F}_+ versus (a) the maximum driving detuning Δ_{Max} for $P_{\text{Max}} = 750 \,\mu\text{W}$ and (b) the maximum driving power P_{Max} for $\Delta_{\text{Max}} = -290 \,\text{kHz}$, by executing a closed

control loop. Two insets show how the loops vary along the horizontal axis of each panel, and the black crosses indicate the location of the EP. \mathbf{c} , \mathbf{d} Imposing topological operations in (\mathbf{c}) \mathcal{DMN} and (\mathbf{d}) \mathcal{DMB} regimes enables TPB and TPT, respectively.

counterintuitive path starting on one sheet but ending on the other, giving rise to TPT. Our study sheds light on the synergy of dark-mode engineering and topological operations, offers an unconventional tool for tasks that cannot be executed by conventional topological mechanisms, and benefits for implementing dark-mode-free topological physics.

TPB and TPT enabled by dark-mode engineering

The TPT efficiency \mathbf{F}_+ is plotted versus Δ_{Max} and P_{Max} in both \mathcal{DMN} ($g_2 = g_1$, $\xi/\omega_m = 5 \times 10^{-4}$, and $\Theta = 0$) and \mathcal{DMB} ($g_2 = 2.76g_1$, $\xi/\omega_m = 5 \times 10^{-4}$, and $\Theta/\pi = 1/9$) regimes, as shown in Figs. 3a, b and Supplementary Fig. S4. We reveal that in the \mathcal{DMN} regime, TPB occurs ($\mathbf{F}_+ = 0$, blue dashed horizontal lines); while in the \mathcal{DMB} regime, an excellent TPT emerges ($\mathbf{F}_+ = 1$, red solid curves). Specifically, in the \mathcal{DMN} regime, thermal phonons concealed in the dark mode that is decoupled from the system cannot be transferred to the bright mode regardless of the tuning of the system parameters, giving rise to TPB [Fig. 3c]. In stark contrast to this, in the \mathcal{DMB} regime, an efficient extraction of thermal phonons is achieved, yielding TPT [Fig. 3d]. These findings demonstrate that leveraging the dark-mode control enabled by synthetic magnetism not only establishes a flexible switch between TPB and TPT, but also provides the possibility of immunizing all topological quantum resources against various dark-mode disturbances in practical devices.

Physically, in conventional schemes (i.e., without synthetic magnetism), topological behavior is inherently fragile to dark modes decoupled from the system, leading to a complete malfunction of both EPs and topological operations^{24,25}. However, by employing synthetic magnetism, all topological responses are immune to these dark modes, resulting in the function of topological operations. Our approach offers a way of enabling practical dark-mode-sensitive quantum setups to be effectively ideal, beneficial for achieving dark-mode-immune topological resources.

Dark-mode-engineered nonreciprocal topology

To study the dependence of one-way topological dynamics on dark-mode engineering, we display the TPT efficiency versus the duration τ of the closed control loops, when the system operates in both \mathcal{DMN} ($g_2 = g_1$, $\xi/\omega_m = 5 \times 10^{-4}$, and $\Theta = 0$) and \mathcal{DMB} ($g_2 = 2.76g_1$, $\xi/\omega_m = 5 \times 10^{-4}$, and $\Theta/\pi = 1/9$) regimes, as shown in Fig. 4 and Supplementary Fig. S5. In the \mathcal{DMN} regime, TPB always happens (i.e., $\mathbf{F}_+ = 0$) no matter how to execute the control loops in parameter spaces (see lower blue and red solid horizontal lines). In the \mathcal{DMB} regime, by rapidly winding around the EP (i.e., $\tau \to 0$), TPB (i.e., $\mathbf{F}_+ \to 0$) is observed; while with adiabatically encircling this EP (i.e., $\tau \to 1$ ms), an excellent TPT is achieved (i.e., $\mathbf{F}_+ \to 1$). These findings demonstrate that the vanishing TPT, corresponding to the emergence of TPB, results from either the dark mode in the \mathcal{DMN} regime or a rapid encirclement of the EP in the \mathcal{DMB} regime.

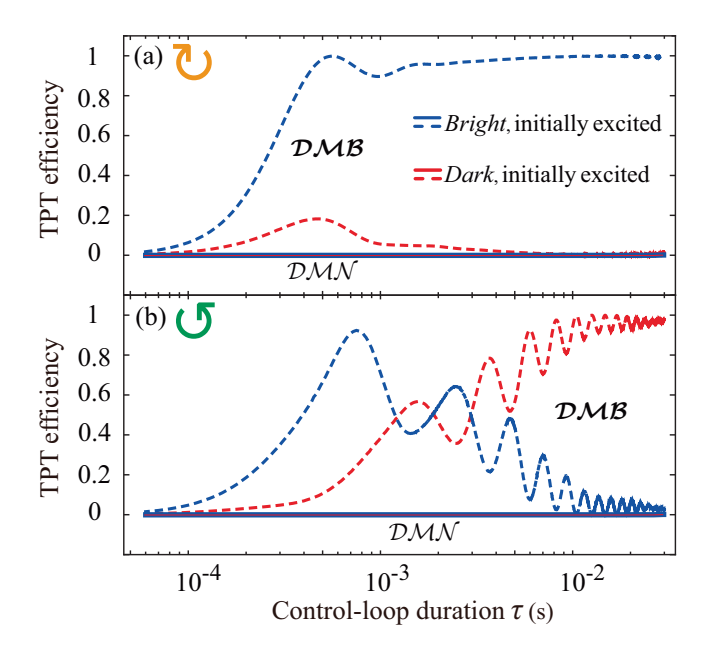


Fig. 4 | **Nonreciprocal topological dynamics via dark-mode engineering.** TPT efficiency versus the duration τ of a closed control loop, in both \mathcal{DMN} and \mathcal{DMB} regimes. The control-loop shape enclosing an EP is the same for all data series, and this EP is encircled in (a) clockwise and (b) counterclockwise directions. Blue or red curves correspond to the data where the bright or dark mode is initially excited, respectively.

By adiabatically winding around the EP, the TPT limiting behavior is contingent upon both the direction of the control loop and the mode initially excited. For example, by executing a clockwise (counterclockwise) loop, the blue (red) curves represent conventional adiabaticity (i.e., the efficiency becomes 1 with τ); while the red (blue) curves show the opposite behavior (i.e., the efficiency becomes 0 with τ). These results prove that, in general, the dark-mode engineering can achieve the nonreciprocity of each topological operation for an anti-clockwise or clockwise control loop enclosing an EP.

For example, when the dark mode is initially excited and the system operates in the \mathcal{DMB} regime, we reveal that adiabatically encircling an EP in the counterclockwise direction gives rise to an excellent TPT [$\mathbf{F}_+ \rightarrow 1$, see the red dashed curve in Fig. 4b], but not in the clockwise sense [$\mathbf{F}_+ \rightarrow 0$, see the red solid curve and symbols in Fig. 4a]. Physically, adiabatic behavior occurs when the system operates only in the less-damped eigenmode. This is because when working in the more-damped mode, the fierce competition between the differential-loss effect (that is exponentially large in τ) and the

nonadiabatic transfer (which is exponentially small in τ) results in a breakdown of adiabaticity, which causes the system to eventually relax to the less-damped mode. Such a process can also be interpreted as a manifestation of the Stokes phenomenon of asymptotics.

Scalable network-based TPT and quantum collective groundstate preparation

The proposed dark-mode-engineering mechanism is very general, and can be generalized to quantum optomechanical networks, where $N \ge 3$ phonon modes are coupled to a shared photon mode through optomechanical coupling, $\mathcal{H}_{omc} = \sum_{j=1}^N g_j a^\dagger a (b_j + b_j^\dagger)$, and the nearest-neighbor phonon modes are coupled to each other via phase-dependent phonon-hopping interactions, $\mathcal{H}_{phi} = \sum_{j=1}^{N-1} \xi_j (e^{i\Theta_j} b_j^\dagger b_{j+1} + \text{H.c.})$ (see Supplementary Information). It has been demonstrated that these modulation phases are governed by the term $\sum_{j=1}^{N-1} \Theta_{\nu}$ ($j \in [2, N]$) (see Supplementary Information for detailed derivations), and hence we can safely assume $\Theta_1 = \pi$ and $\Theta_{j \in [2, N-1]} = 0$.

In the absence of synthetic magnetism (i.e., $\xi_j = 0$), only a single bright mode coupled to the system is induced,

$$\mathcal{B} = \sum_{j=1}^{N} \delta b_j / \sqrt{N}, \ bright \ mode, \tag{7}$$

and N-1 dark modes decoupled from the system emerge. Surprisingly, synthetic gauge fields (i.e., $\xi_j \neq 0$ and $\Theta_1 \neq 2n\pi$), induced by the phase-dependent loop-coupling quantum networks, can lead to a simultaneous breaking of all N-1 dark modes (see Supplementary Information for detailed derivations), offering an exciting opportunity of switching quantum networks between the \mathcal{DMN} and \mathcal{DMB} regimes. Therefore, thermal phonons from the dark to bright modes are blockaded in the \mathcal{DMN} regime, but transferred in the \mathcal{DMB} regime, making TPT feasible in quantum networks. These findings demonstrate that the scalable network-based TPT, with immunity against dark modes, can be achieved just by applying dark-mode engineering to quantum networks.

The framework developed here introduces a versatile strategy with wide-ranging implications in quantum physics. Specifically, it can be broadly applied to steer quantum collective motion in macroscopic mechanical systems. Quantum control of collective phonon modes in large-scale mechanical resonators represents an emerging research

frontier⁴⁰. The proposed dark-mode engineering can contribute a powerful and widely applicable tool for this growing field. For example, the recent breakthrough experiment⁴⁰ highlights a key limitation in observing quantum collective motion in macroscopic mechanical resonators: Only a single bright mode can be cooled to its quantum ground state, while all N-1 dark modes remain entirely uncooled. This inherent decoupling of all dark modes from the system renders the dark modes inaccessible to conventional quantum control and ground-state preparation. Building on this pioneering work⁴⁰, our study fundamentally overcomes this constraint by introducing a darkmode engineering mechanism that enables simultaneous ground-state preparation of both bright and dark modes. By simply activating synthetic magnetism, our scheme unlocks the full quantum potential of collective phononic dynamics. It establishes a paradigm in quantum optomechanics that is no longer bound by the limitations imposed by dark modes.

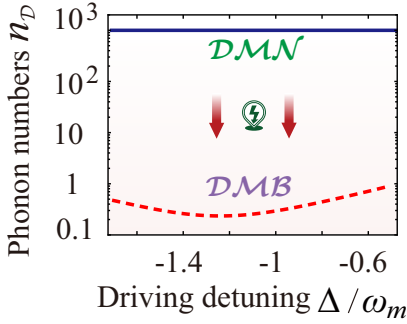
In the \mathcal{DMN} regime, all dark modes remain uncooled $(n_{\mathcal{D}}=10^3)$; whereas in the \mathcal{DMB} regime, they are simultaneously cooled to their quantum ground states $(n_{\mathcal{D}}<1)$, as shown in Fig. 5a. Note that for clarity and brevity, detailed analytical derivations of the final phonon occupations of all dark and bright modes are presented in Section V of Supplementary Information. Physically, thermal phonons trapped in dark modes that are naturally decoupled from the system cannot be extracted through optomechanical sideband cooling⁶⁸⁻⁷¹, making ground-state preparation of all dark modes unattainable⁴⁰. In stark contrast, upon transitioning into the \mathcal{DMB} regime, simultaneous ground-state preparation of all dark and bright modes becomes achievable near the red-sideband resonance ($\Delta/\omega_m = -1$). These results suggest that dark-mode engineering offers flexible control and effective protection of fragile quantum collective ground states.

General dark-state control in quantum optics

Universal dark-state control in quantum optics

Our dark-mode engineering mechanism is highly versatile, offering a robust framework for controlling a wide range of physical phenomena associated with dark states. To clarify this, we reveal the physical mechanism responsible for breaking the dark-state effect in Λ -type three-level systems, by introducing a phase-dependent transition (i.e., the phase in a loop-coupling configuration leads to synthetic magnetism) between the two lower levels [see Fig. 5(b)]. It is well established that in a Λ -type three-level system under two-photon resonance, a dark state emerges, characterized by the zero value of the superposition coefficient associated with the excited state.





(b) $E_e \frac{\Delta_1}{\Delta_1} \frac{\Delta_2}{\Delta_2} |e\rangle$ $\Omega_1 \omega_1 \frac{\Omega_2}{\Omega_b e^{i\Theta}} |f\rangle E_f$ $E_g, |g\rangle \omega_b \omega_b$ $\Theta = n\pi: \text{ dark state}$

 $\Theta \neq n\pi$: dark state **breaking**

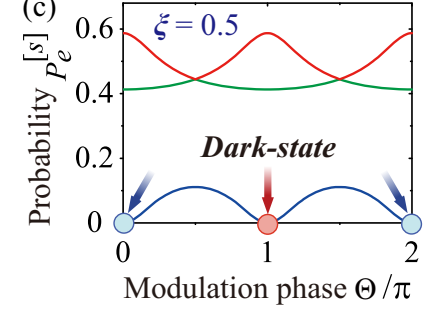


Fig. 5 | Quantum collective ground-state preparation and general dark-state control. a Effective mean phonon number $n_{\mathcal{D}}$ of all N-1 dark modes versus the driving detuning Δ in the \mathcal{DMN} ($\xi_j=0$)⁴⁰ and \mathcal{DMB} ($\xi_j/\omega_m=0.05$, $\Theta=\Theta_1=\pi/2$, $\Theta_{j\in[2,\ N-1]}=0$) regimes. Here we consider the case of N=4 and set $\omega_j/\omega_m=1$, $G_j/\omega_m=0.1$, $\kappa/\omega_m=0.2$, $\gamma_j/\omega_m=10^{-6}$, and $\bar{n}_{\rm th}=10^3$. **b** Schematic diagram of a three-level system with states $|g\rangle$, $|f\rangle$, and $|e\rangle$, corresponding to their energies E_g , E_f , and E_e . Atype coupling configuration involving the transition processes $|g\rangle \rightarrow |e\rangle$ and $|f\rangle \rightarrow |e\rangle$, with detunings $\Delta_{j=1,2}$ and coupling strengths $\Omega_{j=1,2}$. A phase-dependent

resonance interaction with strength $\Omega_b e^{i0}$ between two lower states $(|g\rangle)$ and $|f\rangle)$ is utilized to induce synthetic magnetism, which engineers the dark-state effect, exhibited by the Λ -type three-level system in the two-photon resonance regime $(\Delta_1 = \Delta_2 = \Delta)$. \mathbf{c} Probability $P_e^{[s]}$ of the excited state $|e\rangle$ in the eigenstates $|\lambda_s\rangle$ versus the modulation phase Θ when $\xi = 0.5$. Clearly, the excited-state probability of one of the three eigenstates is zero $(P_e^{[s]} = 0)$ at $\Theta = n\pi$, indicating the emergence of a dark state, and this dark-state effect can be flexibly broken $(P_e^{[s]} \neq 0)$ by tuning $\Theta \neq n\pi$.

In a typical natural atom, direct transitions between the two lower states in a Λ -type three-level system are forbidden by selection rules. However, such transitions become feasible in artificial cyclic three-level systems or through indirect coupling mechanisms. Accordingly, the Hamiltonian of the system is expressed as

$$\begin{split} \mathcal{H} &= E_{e}|e\rangle\langle e| + E_{f}|f\rangle\big\langle f| + E_{g}|g\rangle\big\langle g| + \Omega_{1}\big(|e\rangle\big\langle g|e^{-i\omega_{1}t} \\ &+ |g\rangle\langle e|e^{i\omega_{1}t}\big) + \Omega_{2}(|e\rangle\big\langle f|e^{-i\omega_{2}t} + |f\rangle\langle e|e^{i\omega_{2}t}) \\ &+ \Omega_{b}(|f\rangle\big\langle g|e^{i\Theta}e^{-i\omega_{b}t} + |g\rangle\big\langle f|e^{-i\Theta}e^{i\omega_{b}t}), \end{split} \tag{8}$$

where E_g , E_f , and E_e are the energy of the three energy levels, i.e., $|g\rangle$, $|f\rangle$, and $|e\rangle$, respectively. The two monochromatic fields with the driving frequencies ω_1 and ω_2 are, respectively, coupled to the atomic transitions $|g\rangle \rightarrow |e\rangle$ and $|f\rangle \rightarrow |e\rangle$, with Ω_1 and Ω_2 being the corresponding real transition amplitudes. In such a system, we introduce the transition detunings as $\Delta_1 = E_e - E_g - \omega_1$ and $\Delta_2 = E_e - E_f - \omega_2$, which are related to the two transitions $|g\rangle \rightarrow |e\rangle$ and $|f\rangle \rightarrow |e\rangle$, respectively.

Clearly, we see that a dark state is possessed by the Λ -type coupling system, when the two-photon resonance $(\Delta_1 = \Delta_2 = \Delta)$ is fulfilled for the transitions. To illustrate the dark-state breaking, we introduce a resonance field that couples the two lower states, i.e., $|f\rangle$ and $|g\rangle$. Notably, this coupling features a phase-dependent strength, which induces synthetic magnetism, serving as the critical factor that enables the breaking of the dark state. In a rotating frame with respect to $H_0 = (E_g + \omega_1)|e\rangle\langle e| + E_f |f\rangle\langle f| + E_g |g\rangle\langle g|$, the the system Hamiltonian becomes

$$V_{I} = \Delta |e\rangle \langle e| + \Omega_{1}(|e\rangle \langle g| + |g\rangle \langle e|) + \Omega_{2}(|e\rangle \langle f| + |f\rangle \langle e|) + \Omega_{b}(|f\rangle \langle g|e^{i\Theta} + |g\rangle \langle f|e^{-i\Theta}).$$
(9)

By defining three basis states via the following vectors:

$$|e\rangle = (1, 0, 0)^T, |f\rangle = (0, 1, 0)^T, |g\rangle = (0, 0, 1)^T,$$
 (10)

the interaction Hamiltonian in Eq. (9) becomes

$$\mathcal{V}_{I} = \Omega \begin{pmatrix} 0 & 1 & 1 \\ 1 & 0 & \xi e^{i\Theta} \\ 1 & \xi e^{-i\Theta} & 0 \end{pmatrix}, \tag{11}$$

where $\xi = \Omega_b/\Omega$. Without loss of generality, we have considered the symmetric coupling case $(\Omega_1 = \Omega_2 = \Omega)$ as well as the conditions of single-photon and two-photon resonance $(\Delta_1 = \Delta_2 = \Delta = 0)$. Then we obtain the eigenequation $\frac{1}{\Omega} \mathcal{V}_I | \lambda_s \rangle = \lambda_s | \lambda_s \rangle$, where λ_s are the eigenvalues, determined by the secular (cubic) equation

$$\lambda^{3} - (2 + \xi^{2})\lambda - 2\xi\cos\Theta = 0.$$
 (12)

The solutions to Eq. (12) are then obtained using the Cardano formula, and the eigenstates can be expressed as:

$$|\lambda_s\rangle = c_g^{[s]}|g\rangle + c_f^{[s]}|f\rangle + c_e^{[s]}|e\rangle, \ s=1,2,3. \tag{13}$$

The dark state can be verified by calculating the probability amplitude $P_e^{[s]}$ of the excited state $|e\rangle$ within these eigenstates:

$$P_e^{[s]} = |\langle e|\lambda_s\rangle|^2 = |c_e^{[s]}|^2 \begin{cases} = 0, Dark \text{ state,} \\ \neq 0, Bright \text{ state,} \end{cases}$$
(14)

where $P_e^{[S]}=0$ and $P_e^{[S]}\neq 0$ correspond to the emergence of the dark and bright states, respectively. Specifically, we present the probability $P_e^{[S]}$ of the excited state $|e\rangle$ in the three eigenstates $|\lambda_s\rangle$ versus the modulation phase Θ , for a fixed value of ξ , as depicted in Fig. 5c. We observe that one of the eigenstates becomes a dark state $(P_e^{[S]}=0)$ when $\Theta=n\pi$,

while no dark states emerge in other cases $(P_e^{[s]} \neq 0)$. It demonstrates that by tuning $\Theta \neq n\pi$, the dark-state effect can be broken on demand. Therefore, the phase-dependent resonant transition $|g\rangle \leftrightarrow |f\rangle$, yielding synthetic magnetism, can be utilized to break the dark-state effect in the Λ -type three-level system. Our findings could advance the development of scalable quantum information processors utilizing photons and phonons, with potential applications in state or energy manipulation, photon or phonon pulse generation, quantum repeaters, and the conversion of information between excitations $^{64-67}$.

Proposed experimental implementations

The proposed physical model is general and, in principle, can be implemented using standard optomechanical platforms. Realizing the TPT while maintaining immunity against dark modes requires two key ingredients: in-parallel optomechanical couplings between multiple phonon modes and a shared photon mode, and phase-dependent phonon-hopping interactions between the nearest-neighbor phonon modes. Both types of interactions must be accessible within viable experimental platforms. While each type of coupling has been demonstrated independently in previous experiments, their simultaneous implementation within the same experimental setup has not yet been reported. Nevertheless, under current state-of-the-art experimental conditions, integrating both kinds of interactions into a unified system appears fully feasible.

Recent advances have enabled the experimental realization of inparallel optomechanical couplings between multiple phonon modes and a shared photon mode in both optical^{24,72,73} and microwave⁷⁴⁻⁷⁸ domains. In the optical regime, these in-parallel optomechanical couplings are implemented via "membrane-in-the-middle" optomechanical architectures^{24,72,73}; whereas in the microwave domain, they are realized using circuit electromechanical platforms⁷⁴⁻⁷⁸. Simultaneously, the phase-dependent phonon-hopping interaction between the nearest-neighbor phonon modes can be implemented using photonic-crystal optomechanical platforms⁵⁴ or circuit electromechanical systems⁷⁴⁻⁷⁹. In photonic-crystal-based implementations, this phase-dependent coupling arises from the mediation of two auxiliary cavity fields⁵⁴; whereas in circuit electromechanical systems, it emerges indirectly through the coupling of two mechanical resonators to a charge qubit.

(i) Building on these state-of-the-art experimental advances in both parallel optomechanical couplings and phase-dependent phonon-hopping interactions, the proposed model can be easily realized using photonic-crystal optomechanical architectures featuring optical and mechanical couplings between two optomechanical cavities⁵⁴. In this scheme, each cavity is driven by a distinct phase-correlated laser field, and the effective implementation of our model emerges through the adiabatic elimination of any one cavity-field mode under the largedetuning regime³⁹. Specifically, we consider a multimode physical system featuring both optical and mechanical interactions between the two optomechanical cavities. In the large-detuning regime of the cavity mode, this mode can be adiabatically eliminated, yielding an effective three-mode phase-dependent loop-coupled Hamiltonian³⁹. where both the proposed model and the resulting synthetic magnetism can be easily realized under state-of-the-art experimental conditions using photonic-crystal optomechanical-cavity systems⁵⁴.

(ii) Moreover, the proposed model can be readily implemented using circuit electromechanical platforms^{74–79}, which comprise N micromechanical resonators (MRs) (i.e., $b_{j=1...N}$) coupled to a microwave cavity characterized by an equivalent inductance L and capacitance C. In this quantum setup, the displacement $x_{j=1...N}$ of each MR independently modulates the total capacitance via $C_{j=1...N}(x_j)$, thereby tuning the cavity resonance frequency ω_c . This modulation interaction gives rise to an electromechanical coupling described by $g_{j=1...N} = (\omega_c/2C)\partial C_j(x_j)/\partial x_j$, enabling the precise quantum control over the system's dynamics. Meanwhile, an effective phase-dependent phonon-hopping

interaction between the two nearest-neighbor MRs is induced by the coupling of the two MRs to a superconducting charge qubit³⁹. It reveals that an effective phase-dependent phonon-hopping interaction emerges between the two nearest-neighbor MRs and then, the modulation phase in the loop-coupling configuration induces synthetic magnetism. These findings highlight the direct relevance of the proposed phenomena to state-of-the-art experiments in circuit electromechanical systems, suggesting that current experimental capabilities are sufficient to realize the proposed scheme and that the predicted effects are observable with cutting-edge implementations.

Building on the insightful observation that synthetic magnetic fields provide a powerful route to engineering gauge potentials for photons, we highlight the growing interest in photonic synthetic dimension platforms⁶⁰. These platforms not only enable strong photon-photon interactions but also naturally facilitate the realization of synthetic magnetic fields⁶⁰⁻⁶³. Specifically, the synthetic magnetic field significantly aids the generation of gauge potentials for photons. Recent advances have generated intense interest in photonic platforms with synthetic dimensions⁶⁰, which enable strong photonphoton interactions and synthetic magnetic fields⁶⁰⁻⁶³. These developments highlight the significant potential for realizing our theoretical proposal within synthetic-dimensional photonic systems. Importantly, the proposed dark-mode-engineering mechanism could be easily transferred to chip-based platforms, marking a significant step toward scalable quantum information processing. This prospect is particularly exciting, as it offers a practical pathway to integrate topological photonic or phononic functionalities into compact, chip-scale architectures.

Discussion

Optomechanical dark modes, analogous to the coherent-population trapped state or dark state in atomic physics^{80,81}, can be broadly classified into two categories: optical dark modes and mechanical dark modes. Specifically, optical dark modes arise from the coupling of two optical modes to a shared mechanical mode⁶⁵⁻⁶⁷, while mechanical dark modes emerge from the coupling of two mechanical modes to a common optical mode³⁵⁻⁴⁰. Notably, prior demonstrations⁶⁵⁻⁶⁷ focus on optical dark modes that enable optical mode conversion, whereas our work focuses on mechanical dark modes that suppress mechanical mode conversion.

The phonon-mediated and photon-mediated processes, which respectively correspond to the optical and mechanical mode conversions, can be pursued using multimode optomechanical systems. However, the influence of optomechanical dark modes on these two conversions differs fundamentally. In the previous studies⁶⁵⁻⁶⁷, an optical dark (bright) mode, formed by a special coherent superposition of two optical modes, is decoupled from (coupled to) the mechanical mode. Consequently, the formation of the optical dark mode serves as a shield, protecting the system from mechanical dissipation. Despite being decoupled, the optical dark mode can still mediate an effective interaction between the two optical modes, thereby facilitating the optical-field conversion between them. Moreover, the presence of the optical dark mode enables a phononmediated coupling (which is immune to thermal mechanical motion) for various quantum applications, thereby eliminating the need for quantum ground-state cooling of the mechanical resonator. In our work, the mechanical dark mode emerges as a distinct coherent superposition of two mechanical modes coupled to a common cavity mode. The interference-induced cancellation in coupling effectively decouples the mechanical dark mode from the system. While this decoupling still permits an effective interaction between the two mechanical modes, both mechanical mode conversion and topological phonon transfer between mechanical dark and bright modes become fundamentally suppressed, regardless of adiabatic trajectory design or system parameter tuning. The underlying physical mechanism of this

counterintuitive phenomenon is due to dark-mode-induced disruption of both topological operations and EPs. Here, we address this long-standing challenge posed by mechanical dark modes and demonstrate a fundamentally distinct one-way topological phonon transfer, revealing an unexpected immunity to dark-mode-induced obstruction. This robustness arises from the interplay between topological operations and synthetic magnetism, enabling a controlled transition between the \mathcal{DMN} and \mathcal{DMB} regimes.

In a general topological system, the emergence of an EP signals a transition in the system's topological phase as a function of the parameter space. This transition is often accompanied by a change in the system's topological invariants, such as the conversion from a topologically trivial to a topologically nontrivial state⁸². However, these behaviors always occur in the traditional energy-band topology, involving non-Hermitian gap structures82. In this work, we focus on a three-mode optomechanical system consisting of two mechanical modes coupled to a shared cavity-field mode. By adiabatically eliminating the cavity-field mode, we obtain an effective non-Hermitian Hamiltonian for the two mechanical modes. In this system, topological operations encircling an EP enable nonreciprocal phonon transfer between two mechanical normal modes. Note that our system is a unique non-Hermitian gapless structure, and the traditional concept of energy-band topology is not directly applicable to our studied system. This indicates that the system is fundamentally different from the one investigated in our work, as our focus is exclusively on the non-Hermitian gapless structure rather than on the gap structure. Therefore, the transition from a topologically trivial to a nontrivial state, which happens in the traditional energy-band topology, lies beyond the scope of our system.

In conclusion, we demonstrated a versatile switch between TPB and TPT arising from a general dark-mode engineering, without which it vanishes. Our study differs from what is known in previously established demonstrations, mainly because we are focused on overcoming the challenge from dark-mode contamination in topological responses, but not on deliberately circumventing it. The proposed physical mechanism is highly universal, thereby enabling the control of a wide range of physical effects associated with dark states. Our work presents a comprehensive approach to engineering and protecting topological resources from both dark modes and dark states, providing a perspective on the construction of an unconventionally non-reciprocal topology with immunity to dark modes.

Data availability

The authors declare that the data supporting the findings of this study are available within the paper and its supplementary information files.

Code availability

The code used for the current study is available from the corresponding author on reasonable request.

References

- 1. Kato, T. Perturbation Theory for Linear Operators (Springer, 2013).
- 2. Heiss, W. D. Phases of wave functions and level repulsion. *Eur. Phys. J. D.* **7**, 1 (1999).
- El-Ganainy, R. et al. Non-Hermitian physics and PT symmetry. Nat. Phys. 14, 11 (2018).
- Parto, M., Liu, Y. G. N., Bahari, B., Khajavikhan, M. & Christodoulides, D. N. Non-Hermitian and topological photonics: optics at an exceptional point. *Nanophotonics* 10, 403 (2021).
- Makris, K. G., El-Ganainy, R., Christodoulides, D. N. & Musslimani, Z. H. Beam dynamics in PT symmetric optical lattices. Phys. Rev. Lett. 100, 103904 (2008).
- Klaiman, S., Günther, U. & Moiseyev, N. Visualization of branch points in PT-symmetric waveguides. Phys. Rev. Lett. 101, 080402 (2008).

- Zheng, M. C., Christodoulides, D. N., Fleischmann, R. & Kottos, T. PT optical lattices and universality in beam dynamics. Phys. Rev. A 82, 010103 (2010).
- Bender, C. M. & Boettcher, S. Real spectra in non-Hermitian Hamiltonians having PT symmetry. Phys. Rev. Lett. 80, 5243 (1998).
- Bender, C. M. Making sense of non-Hermitian Hamiltonians. Rep. Prog. Phys. 70, 947 (2007).
- Khanikaev, A. B. et al. Photonic topological insulators. Nat. Mater. 12, 233 (2013).
- Khanikaev, A. B. & Shvets, G. Two-dimensional topological photonics. Nat. Photonics 11, 763 (2017).
- Jing, H. et al. PT-Symmetric phonon laser. Phys. Rev. Lett. 113, 053604 (2014).
- Özdemir, Ş. K., Rotter, S., Nori, F. & Yang, L. Parity-time symmetry and exceptional points in photonics. Nat. Mater. 18, 783 (2019).
- 14. Pile, F. P. D. Gaining with loss. Nat. Photonics 11, 742 (2017).
- Chen, C., Jin, L. & Liu, R.-B. Sensitivity of parameter estimation near the exceptional point of a non-Hermitian system. N. J. Phys. 21, 083002 (2019).
- Pickup, L., Sigurdsson, H., Ruostekoski, J. & Lagoudakis, P. G. Synthetic band-structure engineering in polariton crystals with non-hermitian topological phases. *Nat. Commun.* 11, 4431 (2020).
- Bergholtz, E. J., Budich, J. C. & Kunst, F. K. Exceptional topology of non-Hermitian systems. Rev. Mod. Phys. 93, 015005 (2021).
- Nair, J. M. P., Mukhopadhyay, D. & Agarwal, G. S. Enhanced sensing of weak anharmonicities through coherences in dissipatively coupled anti-PT symmetric systems. *Phys. Rev. Lett.* 126, 180401 (2021).
- Pino, J. D., Slim, J. J. & Verhagen, E. Non-Hermitian chiral phononics through optomechanically induced squeezing. *Nature* 606, 82 (2022).
- Uzdin, R., Mailybaev, A. & Moiseyev, N. On the observability and asymmetry of adiabatic state flips generated by exceptional points. J. Phys. A 44, 435302 (2011).
- Graefe, E.-M., Mailybaev, A. A. & Moiseyev, N. Breakdown of adiabatic transfer of light in waveguides in the presence of absorption. *Phys. Rev. A* 88, 033842 (2013).
- Choi, Y., Hahn, C., Yoon, J. W., Song, S. H. & Berini, P. Extremely broadband, on-chip optical nonreciprocity enabled by mimicking nonlinear anti-adiabatic quantum jumps near exceptional points. *Nat. Commun.* 8, 14154 (2017).
- Yoon, J. W. et al. Time-asymmetric loop around an exceptional point over the full optical communications band. *Nature* 562, 86 (2018).
- Xu, H., Mason, D., Jiang, L. & Harris, J. G. E. Topological energy transfer in an optomechanical system with exceptional points. *Nature* 537, 80 (2016).
- Doppler, J. et al. Dynamically encircling an exceptional point for asymmetric mode switching. *Nature* 537, 76 (2016).
- Ren, H. et al. Topological phonon transport in an optomechanical system. Nat. Commun. 13, 3476 (2022).
- Hassan, A. U., Zhen, B., Soljačić, M., Khajavikhan, M. & Christodoulides, D. N. Dynamically encircling exceptional points: exact evolution and polarization state conversion. *Phys. Rev. Lett.* 118, 093002 (2017).
- 28. Wang, H., Assawaworrarit, S. & Fan, S. Dynamics for encircling an exceptional point in a nonlinear non-Hermitian system. *Opt. Lett.* **44**, 638 (2019).
- 29. Hassan, A. U. et al. Chiral state conversion without encircling an exceptional point. *Phys. Rev. A* **96**, 052129 (2017).
- Zhong, Q., Khajavikhan, M., Christodoulides, D. N. & El-Ganainy, R. Winding around non-Hermitian singularities. *Nat. Commun.* 9, 4808 (2018).
- Feilhauer, J. et al. Encircling exceptional points as a non-Hermitian extension of rapid adiabatic passage. *Phys. Rev. A* 102, 040201(R) (2020).
- Nasari, H. et al. Observation of chiral state transfer without encircling an exceptional point. *Nature* 605, 256 (2022).

- Arkhipov, I. I. et al. Dynamically crossing diabolic points while encircling exceptional curves: A programmable symmetricasymmetric multimode switch. Nat. Commun. 14. 2076 (2023).
- 34. Lai, D.-G., Miranowicz, A. & Nori, F. Nonreciprocal topological phonon transfer independent of both device mass and exceptional-point encircling direction. *Phys. Rev. Lett.* **132**, 243602 (2024).
- 35. Genes, C., Vitali, D. & Tombesi, P. Simultaneous cooling and entanglement of mechanical modes of a micromirror in an optical cavity. *N. J. Phys.* **10**, 095009 (2008).
- 36. Shkarin, A. B. et al. Optically mediated hybridization between two mechanical modes. *Phys. Rev. Lett.* **112**, 013602 (2014).
- Sommer, C. & Genes, C. Partial optomechanical refrigeration via multimode cold-damping feedback. *Phys. Rev. Lett.* 123, 203605 (2019).
- Lai, D.-G. et al. Nonreciprocal ground-state cooling of multiple mechanical resonators. Phys. Rev. A 102, 011502(R) (2020).
- Lai, D.-G., Liao, J.-Q., Miranowicz, A. & Nori, F. Noise-tolerant optomechanical entanglement via synthetic magnetism. *Phys. Rev. Lett.* 129, 063602 (2022).
- 40. Chegnizadeh, M. et al. Quantum collective motion of macroscopic mechanical oscillators. *Science* **386**, 1383 (2024).
- 41. Kitagawa, T. et al. Observation of topologically protected bound states in photonic quantum walks. *Nat. Commun.* **3**, 882 (2012).
- Malzard, S., Poli, C. & Schomerus, H. Topologically protected defect states in open photonic systems with non-hermitian chargeconjugation and parity-time symmetry. *Phys. Rev. Lett.* 115, 200402 (2015).
- 43. Cardano, F. et al. Statistical moments of quantum-walk dynamics reveal topological quantum transitions. *Nat. Commun.* **7**, 11439 (2016).
- 44. Rechtsman, M. C. et al. Topological protection of photonic path entanglement. *Optica* **3**, 925 (2016).
- Mittal, S., Orre, V. V. & Hafezi, M. Topologically robust transport of entangled photons in a 2D photonic system. *Opt. Express* 24, 15631 (2016).
- 46. Gorlach, M. A. & Poddubny, A. N. Topological edge states of bound photon pairs. *Phys. Rev. A* **95**, 053866 (2017).
- 47. Barik, S. et al. A topological quantum optics interface. Science **359**, 666 (2018).
- 48. Blanco-Redondo, A., Bell, B., Oren, D., Eggleton, B. J. & Segev, M. Topological protection of biphoton states. *Science* **362**, 568 (2018).
- 49. Mittal, S., Goldschmidt, E. A. & Hafezi, M. A topological source of quantum light. *Nature* **561**, 502 (2018).
- 50. Mittal, S., Orre, V. V., Goldschmidt, E. A. & Hafezi, M. Tunable quantum interference using a topological source of indistinguishable photon pairs. *Nat. Photonics* **15**, 542 (2021).
- 51. Schmidt, M., Kessler, S., Peano, V., Painter, O. & Marquardt, F. Optomechanical creation of magnetic fields for photons on a lattice. *Optica* **2**, 635 (2015).
- 52. Shen, Z. et al. Experimental realization of optomechanically induced non-reciprocity. *Nat. Photonics* **10**, 657 (2016).
- Ruesink, F., Miri, M.-A., Alù, A. & Verhagen, E. Nonreciprocity and magnetic-free isolation based on optomechanical interactions. *Nat. Commun.* 7, 13662 (2016).
- 54. Fang, K. et al. Generalized non-reciprocity in an optomechanical circuit via synthetic magnetism and reservoir engineering. *Nat. Phys.* **13**, 465 (2017).
- 55. Bernier, N. R. et al. Nonreciprocal reconfigurable microwave optomechanical circuit. *Nat. Commun.* **8**, 604 (2017).
- 56. Shen, Z. et al. Reconfigurable optomechanical circulator and directional amplifier. *Nat. Commun.* **9**, 1797 (2018).
- 57. Ruesink, F. et al. Optical circulation in a multimode optomechanical resonator. *Nat. Commun.* **9**, 1798 (2018).
- Mathew, J. P., Pino, J. D. & Verhagen, E. Synthetic gauge fields for phonon transport in a nano-optomechanical system. *Nat. Nano*technol. 15, 198 (2020).

- Chen, Y. et al. Synthetic Gauge Fields in a Single Optomechanical Resonator. Phys. Rev. Lett. 126, 123603 (2021).
- Yuan, L., Lin, Q., Xiao, M. & Fan, S. Synthetic dimension in photonics. Optica 5, 1396 (2018).
- 61. Ye, R. et al. Observing non-Hermiticity induced chirality breaking in a synthetic Hall ladder. *Light Sci. Appl.* **14**, 39 (2025).
- Dong, Z. et al. Temporal multilayer structures in discrete physical systems towards arbitrarydimensional non-Abelian Aharonov-Bohm interferences. *Nat. Commun.* 15, 7392 (2024).
- Dong, Z., Chen, X., Dutt, A. & Yuan, L. Topological dissipative photonics and topological insulator lasers in synthetic time-frequency dimensions. *Laser Photonics Rev.* 18, 2300354 (2024).
- 64. Kok, P. et al. Linear optical quantum computing with photonic qubits. *Rev. Mod. Phys.* **79**, 135 (2007).
- Dong, C., Fiore, V., Kuzyk, M. C. & Wang, H. Optomechanical dark mode. Science 338, 1609 (2012).
- Wang, Y.-D. & Clerk, A. A. Using interference for high fidelity quantum state transfer in optomechanics. *Phys. Rev. Lett.* 108, 153603 (2012).
- Tian, L. Adiabatic state conversion and pulse transmission in optomechanical systems. *Phys. Rev. Lett.* 108, 153604 (2012).
- Wilson-Rae, I., Nooshi, N., Zwerger, W. & Kippenberg, T. J. Theory of ground state cooling of a mechanical oscillator using dynamical backaction. *Phys. Rev. Lett.* **99**, 093901 (2007).
- Marquardt, F., Chen, J. P., Clerk, A. A. & Girvin, S. M. Quantum theory of cavity-assisted sideband cooling of mechanical motion. *Phys. Rev. Lett.* 99, 093902 (2007).
- 70. Chan, J. et al. Laser cooling of a nanomechanical oscillator into its quantum ground state. *Nature* **478**, 89 (2011).
- 71. Teufel, J. D. et al. Sideband cooling of micromechanical motion to the quantum ground state. *Nature* **475**, 359 (2011).
- Xu, H., Jiang, L., Clerk, A. A. & Harris, J. G. E. Nonreciprocal control and cooling of phonon modes in an optomechanical system. *Nature* 568, 65 (2019).
- Bhattacharya, M. & Meystre, P. Multiple membrane cavity optomechanics. *Phys. Rev. A* 78, 041801(R) (2008).
- Massel, F. et al. Microwave amplification with nanomechanical resonators. Nature 480, 351 (2011).
- 75. Massel, F. et al. Multimode circuit optomechanics near the quantum limit. *Nat. Commun.* **3**, 987 (2012).
- 76. Ockeloen-Korppi, C. F. et al. Sideband cooling of nearly degenerate micromechanical oscillators in a multimode optomechanical system. *Phys. Rev. A* **99**, 023826 (2019).
- Ockeloen-Korppi, C. F. et al. Stabilized entanglement of massive mechanical oscillators. *Nature* 556, 478 (2018).
- de Lépinay, L. M., Ockeloen-Korppi, C. F., Woolley, M. J. & Sillanpää,
 M. A. Quantum mechanics-free subsystem with mechanical oscillators. Science 372, 625 (2021).
- 79. Liu, Y.-X., You, J. Q., Wei, L. F., Sun, C. P. & Nori, F. Optical selection rules and phase-dependent adiabatic state control in a superconducting quantum circuit. *Phys. Rev. Lett.* **95**, 087001 (2005).
- 80. Arimondo, E. Coherent population trapping in laser spectroscopy. *Prog. Opt.* **35**, 257 (1996).
- 81. Lukin, M. D. Colloquium: trapping and manipulating photon states in atomic ensembles. *Rev. Mod. Phys.* **75**, 457 (2003).
- 82. Kawabata, K., Bessho, T. & Sato, M. Classification of exceptional points and non-Hermitian topological semimetals. *Phys. Rev. Lett.* **123**, 066405 (2019).

Acknowledgements

We gratefully acknowledge Prof. Jie-Qiao Liao for his great help on the analytical derivations and numerical simulations. A.M. is supported by the Polish National Science Centre (NCN) under the Maestro Grant No. DEC-2019/34/A/ST2/00081. F.N. is supported in part by: the Japan Science and Technology Agency (JST) [via the CREST Quantum Frontiers program Grant No. JPMJCR24I2, the Quantum Leap Flagship Program (Q-LEAP), and the Moonshot R&D Grant Number JPMJMS2061], and the Office of Naval Research (ONR) Global (via Grant No. N62909-23-1-2074).

Author contributions

D.G.L. conceived the project and performed calculations. D.G.L., A.M., and F.N. interpreted the results. F.N. supervised the project. All authors contributed in writing the manuscript.

Competing interests

The authors declare no competing interests.

Additional information

Supplementary information The online version contains supplementary material available at https://doi.org/10.1038/s41467-025-63042-9.

Correspondence and requests for materials should be addressed to Deng-Gao Lai.

Peer review information *Nature Communications* thanks Rui Ye, and the other, anonymous, reviewer(s) for their contribution to the peer review of this work. A peer review file is available.

Reprints and permissions information is available at http://www.nature.com/reprints

Publisher's note Springer Nature remains neutral with regard to jurisdictional claims in published maps and institutional affiliations.

Open Access This article is licensed under a Creative Commons Attribution-NonCommercial-NoDerivatives 4.0 International License, which permits any non-commercial use, sharing, distribution and reproduction in any medium or format, as long as you give appropriate credit to the original author(s) and the source, provide a link to the Creative Commons licence, and indicate if you modified the licensed material. You do not have permission under this licence to share adapted material derived from this article or parts of it. The images or other third party material in this article are included in the article's Creative Commons licence, unless indicated otherwise in a credit line to the material. If material is not included in the article's Creative Commons licence and your intended use is not permitted by statutory regulation or exceeds the permitted use, you will need to obtain permission directly from the copyright holder. To view a copy of this licence, visit https://creativecommons.org/licenses/by-nc-nd/4.0/.

© The Author(s) 2025